Open Access Articles

Climate change impacts on wave and surge processes in a Pacific Northwest (USA) estuary

The Faculty of Oregon State University has made this article openly available.
Please share how this access benefits you. Your story matters.

Citation	Cheng, T. K., Hill, D. F., Beamer, J., & García-Medina, G. (2015). Climate change impacts on wave and surge processes in a Pacific Northwest (USA) estuary. Journal of Geophysical Research: Oceans, 120(1), 182-200. doi:10.1002/2014JC010268
DOI	10.1002/2014JC010268
Publisher	American Geophysical Union
Version	Version of Record
Terms of Use	http://cdss.library.oregonstate.edu/sa-termsofuse

AGU PUBLICATIONS

JGR

Journal of Geophysical Research: Oceans

RESEARCH ARTICLE

10.1002/2014JC010268

Climate change impacts on wave and surge processes in a Pacific Northwest (USA) estuary

T. K. Cheng[1], D. F. Hill[1], J. Beamer[2], and G. García-Medina[3]

[1]School of Civil and Construction Engineering, Oregon State University, Corvallis, Oregon, USA, [2]Water Resources Engineering, Oregon State University, Corvallis, Oregon, USA, [3]College of Earth, Ocean, and Atmospheric Science, Oregon State University, Corvallis, Oregon, USA

Key Points:
- Climate change impacts on estuarine hydrodynamics can be directly simulated
- Estuaries show spatial and seasonal variability in total water levels
- For the climate scenario studied, changes in total water levels were modest

Correspondence to:
D. F. Hill,
david.hill@oregonstate.edu

Citation:
Cheng, T. K., D. F. Hill, J. Beamer, and G. García-Medina (2015), Climate change impacts on wave and surge processes in a Pacific Northwest (USA) estuary, *J. Geophys. Res. Oceans*, *120*, 182–200, doi:10.1002/2014JC010268.

Received 25 JUN 2014
Accepted 12 DEC 2014
Accepted article online 18 DEC 2014
Published online 21 JAN 2015

Abstract Total water levels (TWLs) within estuaries are influenced by tides, wind, offshore waves, and streamflow, all of which are uniquely affected by climate change. The magnitude of TWL associated with various return periods is relevant to understanding how the hydrodynamics of a bay or estuary may evolve under distinct climate scenarios. A methodology for assessing the hydrodynamic response of a small estuary under major boundary condition perturbations is presented in this study. The coupled Advanced Circulation (ADCIRC) and Simulating Waves Nearshore (SWAN) model was used to simulate wave and water elevation conditions within Tillamook Bay, OR, USA for two long-term scenarios; 1979–1998 and 2041–2060. The model output provided multidecadal time series of TWLs for statistical analysis. Regional climate data from the North American Regional Climate Change Assessment Program (NARCCAP) were used to drive streamflow modeling (MicroMet/SnowModel/HydroFlow) and meteorological forcing within ADCIRC-SWAN. WAVEWATCH III, which was forced with global climate data from the Community Climate Science Model (CCSM, a contributing model to NARCCAP), was used to produce open boundary wave forcing. Latitudinal and seasonal gradients were found in TWLs associated with varying return periods for both the hindcast and forecast. Changes in TWLs from hindcast to forecast included the sea level rise component and were also modulated by changes in boundary conditions.

1. Introduction

Climate change directly impacts how well estuaries can supply ecological services to humans and wildlife. Estuaries provide critical services such as water filtration and habitat protection for species that have commercial, recreational and cultural significance [*Barbier et al*., 2011]. These shallow-water regions drive local economies for coastal communities, such as commercial or recreational fishing, and also serve as hubs for ship transportation and commerce. The efficacy of strategies to preserve and maintain the well being of an estuarine environment is directly linked to a thorough understanding of the physical processes within the domain and how they may be affected by shifts in climate.

In the Pacific Northwest (PNW) of the USA, the hydrodynamics of estuarine environments are particularly unique given the relative strength of the wave climate compared to the rest of the conterminous United States and the hydrologic character of the region. Analysis of historic buoy data from the National Data Buoy Center shows that average winter significant wave heights in Oregon (OR) and Washington (WA) range from 3 to 4 m, with maximum measured wave heights of 10–12 m. Extreme winds and precipitation characterize the PNW winter season, as a result of atmospheric transport of water vapor flux from the tropical Pacific. Winds are typically directed from the south during winter storm events, generating strong longshore currents on open coast and wind-blown surge and waves within bays. Streamflow is strongly correlated with precipitation, which demonstrates a strong annual maximum in winter and minimum in summer. Large interannual and interdecadal variability are present in the magnitude and duration of precipitation events along the West Coast [*Warner et al*., 2012].

For the PNW, the amount of snow cover and, subsequently, summer streamflow are heavily influenced by winter precipitation trends [*Hamlet et al*., 2005]. Recent studies show a steady temporal decline in snowpack and glacier coverage in western North America [*Schiefer et al*., 2007; *Bolch et al*., 2010]. Climate projections predict wetter winters and drier summers for coastal zones in the PNW, which will unduly affect the hydrologic regime and total river discharge into estuaries [*Mote and Salathé*, 2010]. *Leung et al*. [2004] found that

© 2014. American Geophysical Union. All Rights Reserved.

extreme daily precipitation was enhanced in future climate scenarios. The distribution and time scales of major precipitation events dictates the strength of river currents and the spatial extent to which they leave a "signature" in estuarine morphology.

Recent literature has also focused on the increase in wave heights in the North Pacific, suggesting a possible link between storm-induced waves and warmer water temperatures in the Western Pacific [*Graham and Diaz*, 2001]. For the US West Coast, *Allan and Komar* [2000, 2001] showed that the rate of increase in wave heights varies latitudinally, with little to no increase in the southern coast of California and the greatest increase found for the PNW coast. In a later study, *Allan and Komar* [2006] analyzed decadal trends in buoy records and found that average wave heights were increasing at a rate of 0.03 m yr^{-1}. Wave-current interaction within a bay or sheltered area generates the predominant local circulation patterns, thus impacting pollutant dispersal, temperature and salinity mixing, morphological changes, and other physical processes. *Olabarrieta et al*. [2011] examined wave-current interactions in a mesotidal inlet and found that the breaking-induced radiation stress gradient induced wave setup within the estuary beyond the inlet. Additionally, relative sea level rise in the PNW will shift wave breaking closer to shore, thus impacting the extent of setup and local circulation patterns.

Potential impacts of sea level rise and increasing wave heights on open coast beaches in the PNW, such as intensified beach erosion, are well documented in the literature [*Ruggiero et al*., 2010; *Seymour*, 2011]. However, less is understood about how these same factors, combined with changing streamflow patterns, influence the complex interaction of physical processes in tidal inlets and estuaries. Many previous studies have investigated this problem in only a partial, process-based way. For example, *Kuang et al*. [2014] studied the Yangtze River Estuary, China to examine the effects of various sea level rise scenarios but they did not consider future changes in runoff or wave climate. *Zhong et al*. [2008] studied the effects of sea level rise (SLR) on tides in the Chesapeake Bay and showed that SLR will lead to an amplification of tides. However, the effects of river flow, waves, and winds were not included.

Given that many factors (offshore waves, local waves, winds, tides, and streamflow) affect the hydrodynamics of an estuarine environment, a holistic approach toward modeling climate impacts on estuaries is warranted [*Gallien et al*., 2011]. *Barnard et al*. [2014] recently reported on such an approach for open coast erosion processes. They linked wave, tide, and cross-shore profile models in order to assess present and future coastal hazards. This study focuses on the development of an assessment methodology for climate change impacts on small to medium-size estuaries, where the mix of physical processes is very different from the open coast. A coupled circulation and wave model is used to carry out long-term historical (1979–1998) and future scenario (2041–2060) runs in a representative PNW estuary. Major boundary conditions that drive the physical phenomena present in these environments, such as offshore wave forcing and streamflow, are modeled separately, but consistently, in order to provide the boundary conditions for the circulation-wave model. The model output provides, at very high spatiotemporal resolution, multiple decades of wave parameters, water elevations, and water velocities. Statistical analysis of the total water levels (TWLs) computed from these output data streams yields a nuanced view of wave and circulation processes in estuaries and how these processes may respond to changes in estuarine boundary conditions.

2. Methods

In this section, an overview of the study site and computational model are provided. A comprehensive description of the model boundary conditions is also given.

2.1. Study Site

The climate change impact assessment was carried out for Tillamook Bay, a small estuary located in northwestern Oregon (Figure 1). Most of the estuarine waters are sheltered from open coast wave conditions due to Bayocean Spit, located adjacent to the western perimeter of Tillamook Bay, and a jettied inlet of 350 m width. The bay has relatively shallow bathymetry (average 4.6 m depth), and contains complex bathymetric features, such as mud shoal clusters and tidal flats, which dominate local circulation patterns. At mean sea level (MSL), the total surface area and volume of the estuary are 33 km^2 and 0.15 km^3, respectively.

Other major processes influence the water surface elevation within the bay. Five major watersheds drain from the coastal mountain range into the bay: Miami, Kilchis, Wilson, Trask, and Tillamook. The overall bay watershed is shown in Figure 1c. The Miami, Wilson, and Trask Rivers are all gauged (either presently or

© 2014. American Geophysical Union. All Rights Reserved.

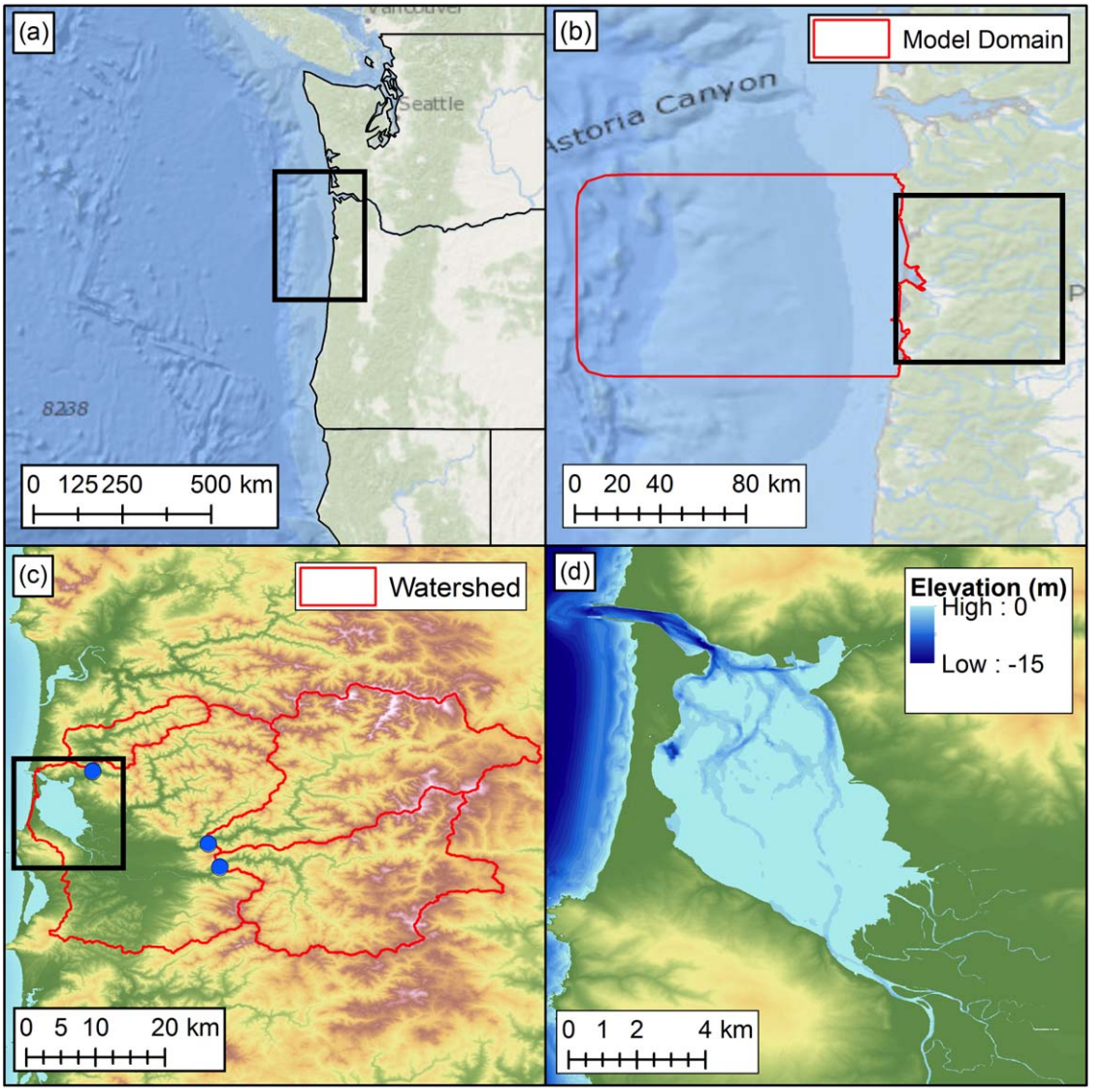

Figure 1. Varying views of the Pacific Northwest coast and the Tillamook Bay region; heavy black lines in Figures 1a–1c show the extent of the subsequent figure. (a) Regional scale view; (b) view showing the extent of the computational model domain; (c) local view showing the full watershed of the estuary. Blue dots indicate USGS gaging stations for the Miami, Trask, and Wilson rivers, whose watersheds lie to the north, northeast, and southeast, respectively; (d) local view showing the bathymetry of Tillamook Bay.

historically) by the United States Geological Survey (USGS). Their gauging station locations and watersheds are all shown in Figure 1c. Collectively, those three watersheds drain 63% of the overall watershed of Tillamook Bay, which has an area of 1400 km^2.

Estuarine conditions reflect a balance between ocean and terrestrial forcing. In a simplistic way, this can be characterized through ratios of relevant volumes. For Tillamook, the tidal prism, which is a proxy for the strength of the tidal forcing, is 0.087 km^3, or roughly half the bay's volume. The annual runoff volume into Tillamook Bay, which is a proxy for the strength of the streamflow forcing, is 3.41 km^3, or roughly twenty times the bay's volume. Latitudinal gradients in precipitation and topographic characteristics produce different ratios of volumes along the western coast of the US. As examples, the Umpqua and Coquille estuaries have runoff to estuary volume ratios in the hundreds.

2.2. Computational Model

The primary models used to model wave and surge climate within Tillamook Bay are the Advanced Circulation (ADCIRC) Shallow Water Model [*Luettich and Westerink*, 1991] and unstructured Simulating Waves

© 2014. American Geophysical Union. All Rights Reserved.

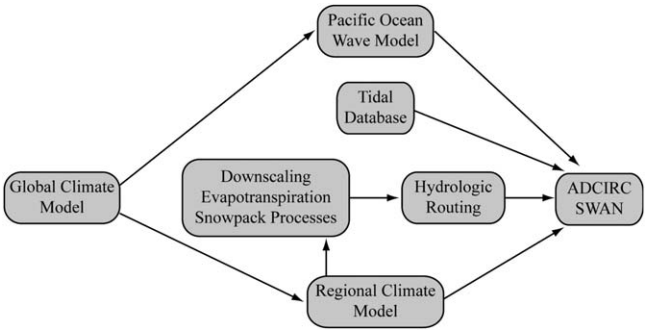

Figure 2. Overview of model flow. Major boundary conditions for ADCIRC-SWAN are developed based off of global and regional climate model output.

Nearshore (SWAN) [*Zijlema*, 2010] Model. Given expected constraints in computational resources and the simulation length of the present study, the 2D depth-integrated (2DDI) barotropic version of the ADCIRC model was selected. The benefits of the recently coupled ADCIRC-SWAN model are twofold: (i) accurate characterization of wave-current interaction in nearshore and coastal areas and (ii) increased computational efficiency since both models utilize a single unstructured mesh [*Dietrich et al*., 2011a]. The development of input boundary conditions to ADCIRC-SWAN using other numerical models is covered in the following sections. The overall model flow is illustrated conceptually in Figure 2.

The 2DDI version of ADCIRC computes water surface elevation, ζ, and depth-integrated velocities, U and V, everywhere on an unstructured grid as solutions to the Generalized Wave-Continuity Equation (GWCE) and depth-averaged momentum equations that include rotation, surface pressure, surface stress, bottom stress, lateral stress gradients, momentum dispersion terms, and baroclinic pressure gradients.

The GWCE is used by ADCIRC in order to avoid spurious oscillations resulting from a primitive Galerkin finite element formulation [*Gray*, 1982]. The optional wetting and drying algorithm within ADCIRC was enabled in this study, such that an element was considered wet if all three vertices composing that particular element had a total water depth exceeding 0.05 m. The nonlinear bottom friction option was used, where a quadratic bottom friction law was applied in deep water and transitioned to a Manning-type friction law as water depth decreased. The reader is referred to the ADCIRC manual for details on calculating bottom friction in shallow water [*Luettich and Westerink*, 2004]. A bottom friction coefficient of $C_f = 0.004$ was specified within the model. Validation runs spanning a wide range of C_f values were carried out and the value of 0.004 provided excellent agreement with tidal gage data (see section 3). A spatially constant horizontal eddy viscosity of 2 $m^2\ s^{-1}$ was used. ADCIRC allows control over whether the GWCE is solved semi-implicitly or explicitly. *Dietrich et al.* [2012a] note that the two methods can have similar time step stability constraints. For the present study, a small $\Delta t = 3$ s was found to be the largest time step to maintain stability everywhere. These parameters were passed to the unstructured version of SWAN at a specified time step of $\Delta t = 600$ s.

SWAN solves the wave action balance equation, given bathymetry, meteorological forcing, water surface elevation and currents, for wave action density [*Booij et al*., 1999]. The formulation allows for action sources like wind-wave growth and sinks, such as whitecapping, bottom friction, and wave breaking. Wave transformation processes, such as shoaling, refraction, and local wave generation by winds are well reproduced in SWAN [*Ris et al*., 1999; *Rogers et al*., 2003]. For the present study, wave frequencies were discretized over 40 bins from 0.031 to 1.42 Hz on a logarithmic scale; direction was binned into 36 intervals of 10° each. Wave radiation stresses were passed back to ADCIRC. Limiters on spectral propagation velocities were introduced for areas of coarse spatial resolution, in order to avoid excessive wave refraction [*Dietrich et al*., 2012b].

The coupled model was run in parallel mode with 192 processors on Lonestar, a Dell Linux computing cluster at the Texas Advanced Computing Center (TACC) at the University of Texas at Austin. The model grid (discussed below) resulted in a computational expense of approximately 2000 core-hours per 1 year of simulation time.

2.3. Grid Development

The ADCIRC-SWAN model was applied to the computational mesh (extent shown in Figure 1b), which extended westward just beyond 125°W longitude. Spatial resolution of mesh elements varied from 4 km at the offshore boundary to 60 m at the coast, adequately resolving the complex bathymetric features such as mud flats and shoals within Tillamook Bay. The final mesh had approximately 55,000 triangular elements and 28,000 nodes.

© 2014. American Geophysical Union. All Rights Reserved.

The mesh bathymetry was based off of coastal relief 1/3 arc sec digital elevation models (DEMs) provided by the NOAA Tsunami Inundation Project for the Garibaldi, OR [*Carignan*, 2009a] and Central Oregon Coast, OR [*Carignan*, 2009b] regions. The 10 m above MSL contour was extracted and used as the model boundary, so that the effects of wetting and drying could be observed. Using the NOAA VDatum tool, the vertical data of all DEMs were transformed from the mean high water (MHW) tidal datum to mean sea level (MSL). Out on Bayocean Spit, more recent USACE LIDAR data from a 2009–2011 survey were given priority [*US Army Corp of Engineers Joint Airborne Lidar Bathymetry Technical Center of Expertise*, 2012].

Relative sea level rise was determined based off of the International Panel of Climate Change A2 emissions scenario *Solomon et al.* [2007]. Although a newer IPCC study has since been published, the climate data (discussed in the following section) chosen to force the models were the only downscaled data set available that covered the entire spatial extent of the domain and that was offered at a subdaily temporal resolution, which is more appropriate than daily values for simulating wave and surge conditions. As the climate data selected were based on the IPCC A2 scenario, a relative sea level rise based upon IPCC A2 was chosen in order to be consistent.

Recent literature has posited that IPCC estimates may be underestimating sea level rise magnitudes [*Rahmstorf et al*., 2012]. *Vermeer and Rahmstorf* [2009] proposed a relationship between global sea level variations and global mean temperature. Based on their results, the historic mesh was lowered (water depth was increased) by 80 cm, a value corresponding to the A2 emissions scenario in the latter 21st century, to account for relative sea level rise over the next several decades.

2.4. Climate Data

Dynamically downscaled global climate data from the North American Regional Climate Change Assessment Program (NARCCAP) [*Mearns et al*., 2009, 2013] were used to drive streamflow modeling and provide meteorological forcing in both the historical (1979–1998) and future (2041–2060) scenarios. NARCCAP is a suite of regional climate models (RCMs) forced by coupled, large-scale atmospheric-ocean general circulation models (AOGCMs). The complete matrix of GCM/RCM pairing features 4 AOGCMs and 6 RCMs, as well as RCMs forced by the National Centers for Environmental Prediction (NCEP)−2 reanalysis data. Boundary conditions driving the AOGCMs for the future period correspond to the SRES A2 emissions scenario [*Solomon et al*., 2007]. Data are offered at a spatial resolution of 50 km and temporal resolution of 3 h. The selection of NARCCAP as this study's regional climate model output was motivated by the combination of high (downscaled from GCM) spatial resolution and high (subdaily) temporal resolution, the latter of which enables more accurate modeling of time-sensitive processes such as local wave generation over several hours. Although other products, such as the Multivariate Adaptive Constructed Analogs (MACA) [*Abatzoglou and Brown*, 2011] data set, offer even finer spatial resolution (4 km) and are based upon more recent CMIP5 multimodel ensembles, the spatial domain does not sufficiently extend offshore of the domain, such that meteorological inputs would not be available. Additionally, MACA is offered at a daily time step, which would act as a low-pass filter and would not fully capture maximum wave heights produced within the bay.

Performing simulations with an ensemble of GCM/RCM pairings is ideal for quantifying the spread in model uncertainty and discerning the extent of climate change impacts [*Burger et al*., 2011; *Elguindi and Grundstein*, 2013; *Miller et al*., 1999]. However, due to limitations in computational resources, only a single GCM/RCM pairing, the Community Climate Science Model/Canadian Regional Climate Model (CCSM/CRCM), was utilized in this study. Previous studies examining the performance of the NARCCAP suite in reproducing climate trends and variability suggested that the selection of GCM/RCM for a regional assessment should be motivated by the strengths and weaknesses of a particular pairing in a geographical area and potential impacts on the physical processes in question [*Pryor et al*., 2006]. Since this study was focused on local wave generation and surge within Tillamook Bay, the veracity of CCSM/CRCM nearsurface wind speeds to historical observations is relevant. *Pryor et al*. [2009] noted that CRCM wind data have the least amount of error relative to other models when compared to in situ observations of extreme wind speeds. Thus, data sets for climate variables: temperature T, precipitation P, wind components u and v, relative humidity ϕ, and surface pressure P_s were extracted from the CCSM/CRCM pairing.

Incorrect initial conditions and mischaracterization of local physics over a grid-scale cell typically seed GCMs with errors, which then propagate through to RCM output and secondary, applied modeling efforts [*Xu*, 1999]. The need to bias correct and statistically downscale GCM data has resulted in a number of methods

© 2014. American Geophysical Union. All Rights Reserved.

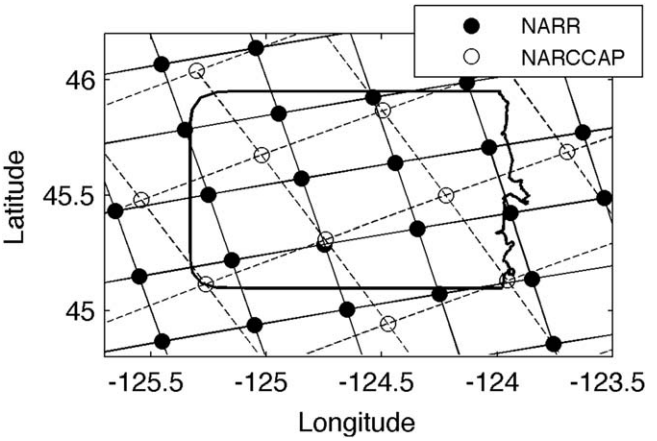

Figure 3. NARR (closed) and NARCCAP (open) grids, at 32 and 50 km spatial resolution, overlaid on the Tillamook Bay computational domain (black outline).

which attempt to bring simulated data in alignment with historical observations [*Boé et al*., 2007; *Chen et al*., 2013; *Haerter et al*., 2011; *Maurer and Hidalgo*, 2008; *Li et al*., 2010]. Similarly, RCM output has been shown to improve in "value" provided when bias-corrected [*Christensen et al*., 2008; *Frei et al*., 2006]. Although the efficacy of bias correction has been heavily debated [*Ehret et al*., 2012], the quantification of uncertainty by using raw output from a suite of GCM/RCM pairings was beyond the scope of this study, thus motivating bias correction and improvement of the quality of the model inputs. A distribution-based quantile mapping method, first proposed by *Panofsky and Brier* [1958] and later expanded on by *Wood et al*. [2004] to include a spatial disaggregation portion, entails replacing a value in the model time series with its corresponding value from a target time series (e.g., observations and reanalysis data) at the same quantile.

Several weather stations exist in the vicinity of Tillamook Bay but none have a consistent, historic record long enough to establish a historical norm for all six climate variables. The dearth of long-term observational data in the region motivated the selection of the NCEP North American Regional Reanalysis (NARR) data set as the target for bias correction [*Mesinger et al*., 2006]. NARR is an extension of the NCEP Global Reanalysis project and offers a variety of climate variables for the current period (1979–present) at 32 km spatial resolution, slightly finer than that of NARCCAP (Figure 3). Since NARR assimilates observational data from a network of weather-observing stations at varying temporal and spatial scales, bias-correcting each raw NARCCAP data set to its corresponding NARR time series should align the former closer to a true historical norm.

Utilizing a distribution-based correction method requires fitting a parametric statistical distribution to each of the climate variables. To preserve seasonal and interannual trends, bias correction was performed on a month-by-month basis. For example, a probability distribution was fitted to values aggregated from January only across the historical period (1979–1998) for both NARR and NARCCAP. Each value corresponds to a quantile, or the inverse of the cumulative distribution function. The raw NARCCAP value was replaced by the NARR value corresponding to the same quantile (Figure 4). This method corrects both the first two statistical moments (mean and variance) in the model data. For example, in Figure 4a, it is observed that the NARCCAP historical data are too cool and have too much variance compared to the NARR data and the bias correction corrects that. Figure 4b shows 1 month of historical time series data. There is no expectation for NARCCAP to exactly match NARR since the former is a model and the latter based on data. However, it is clear that the bias correction step damps out the "too large" variance in the NARCCAP data and produces a time series that is more consistent with the data.

Figure 5 shows climatologies (monthly means) for all of the physical variables extracted from the NARCCAP database. It is clear that the bias correction procedure adequately corrects all variables, with the exception of wind direction. Since the wind components *u* and *v* were corrected independently, the bias in direction was not completely removed. The resultant seasonal trend is still reasonable, however, for the PNW climate.

2.5. Boundary Condition Development

2.5.1. Open Boundary Forcing-Offshore Waves

Future climate change impacts on global and regional waves are also of interest [*Charles et al*., 2012; *Hemer et al*., 2013; *Wang et al*., 2014] and have seen considerable recent study. For the present study, the wave data were generated by implementing WAVEWATCH III v3.14 [*Tolman*, 2002b, hereinafter WW3] at the basin scale (Figure 6). WW3 is a third-generation numerical wave model that has proved skillful for wave

© 2014. American Geophysical Union. All Rights Reserved.

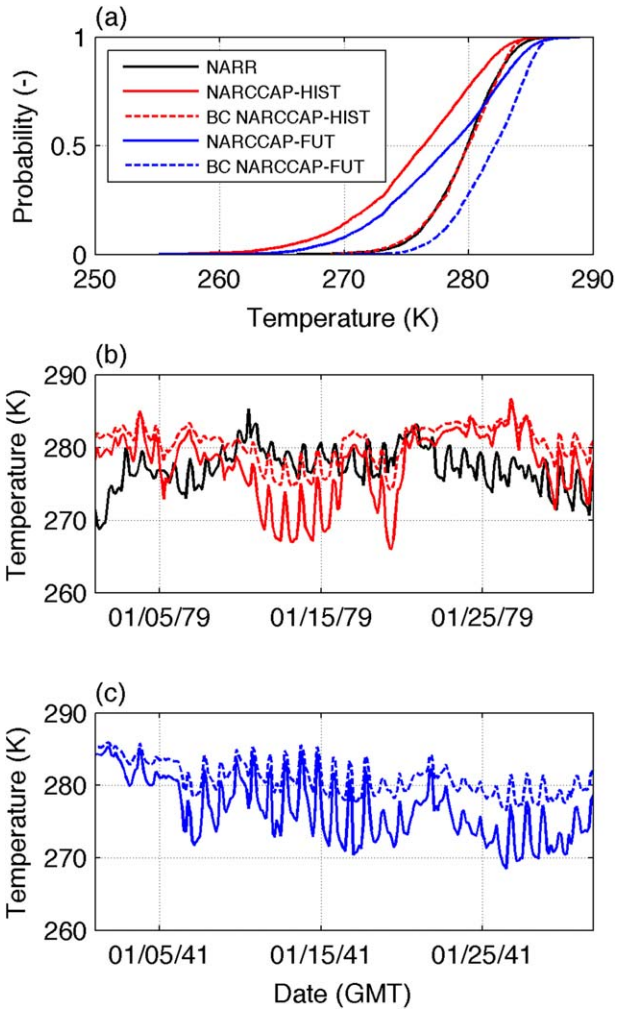

Figure 4. Sample univariate bias correction for temperature, using NARR as a target. (a) Quantile mapping procedure, where the CDF of the historical NARCCAP data set is bias-corrected to match that of the NARR data set; (b) NARR, raw NARCCAP, and bias-corrected NARCCAP data sets for sample historical period; (c) raw NARCCAP and bias-corrected NARCCAP data sets for sample future period.

hindcasting at similar scales in the PNW [*Hanson et al*., 2009]. Like SWAN, it solves the action balance equation, which in this implementation is solved with a third-order propagation scheme [*Tolman*, 2002a]. The numerical simulations were performed over two grids with a spatial resolution of 1° by 1.25° and 0.25° by 0.25° based on NCEP's operational Global and Eastern North Pacific Ocean models, respectively. In this case, the wave frequencies were discretized over 25 logarithmically spaced bins from 0.0418 to 0.411 Hz, while wave directions were binned into 24 intervals of 15° each. The *Tolman and Chalikov* [1996] source term package was used to model wind-wave growth and whitecapping. Nonlinear quadruplet wave interactions were computed with the *Hasselmann et al*. [1985] formulation.

To be consistent with the selection of the CCSM-CRCM GCM/RCM pair, wind data were extracted from the CCSM data set to force WW3. Winds were interpolated to a height of 10 m above mean sea level assuming a stably stratified atmosphere using the 1/7th power law [*Resio et al*., 2008]. Linear interpolation in time and space were performed to match the wind data set with the WW3 nodes and time step. Bias correction of GCM data prior to running the wave model was not possible, since no relevant "targets" exist for NARCCAP grid nodes that span the Pacific Ocean.

WW3 forced with the GCM data resulted in significant overprediction of waves in the PNW, with significant wave heights up to 15 m, warranting bias correction of the output using available observational data. Two buoys off of the northern OR/southern WA coast, Station #46005 (West Washington) and Station #46029 (Columbia River Bar, OR) have long-term wave records that are candidates for capturing the historical wave climate.

The joint modeling of significant wave height (H_s) and mean wave period (T_m) has been well documented in the literature, whether for coastal structure design or wave climate characterization [*Ferreira and Soares*, 2002; *Mathisen and Bitnergregersen*, 1990; *Myrhaug and Hansen*, 1997; *Repko et al*., 2004]. The preservation of the dynamical link between H_s and T_m prevents the generation of unphysical waves, an undesired side effect of independent variable correction. The use of copulas, first described by *Sklar* [1959], allows for the correlation of two or more variables without perturbing the marginal distributions. Copulas have become increasingly used in characterization of sea state in recent literature [*Corbella and Stretch*, 2012; *De Waal and van Gelder*, 2005].

In the weather data bias-correction, the availability of a gridded target (the NARR data) product at a fine resolution was able to resolve any spatial rate of change in bias and subsequent impacts on the degree of error removed. Neither of the wave buoys are located right at the perimeter of the ADCIRC-SWAN mesh

© 2014. American Geophysical Union. All Rights Reserved.

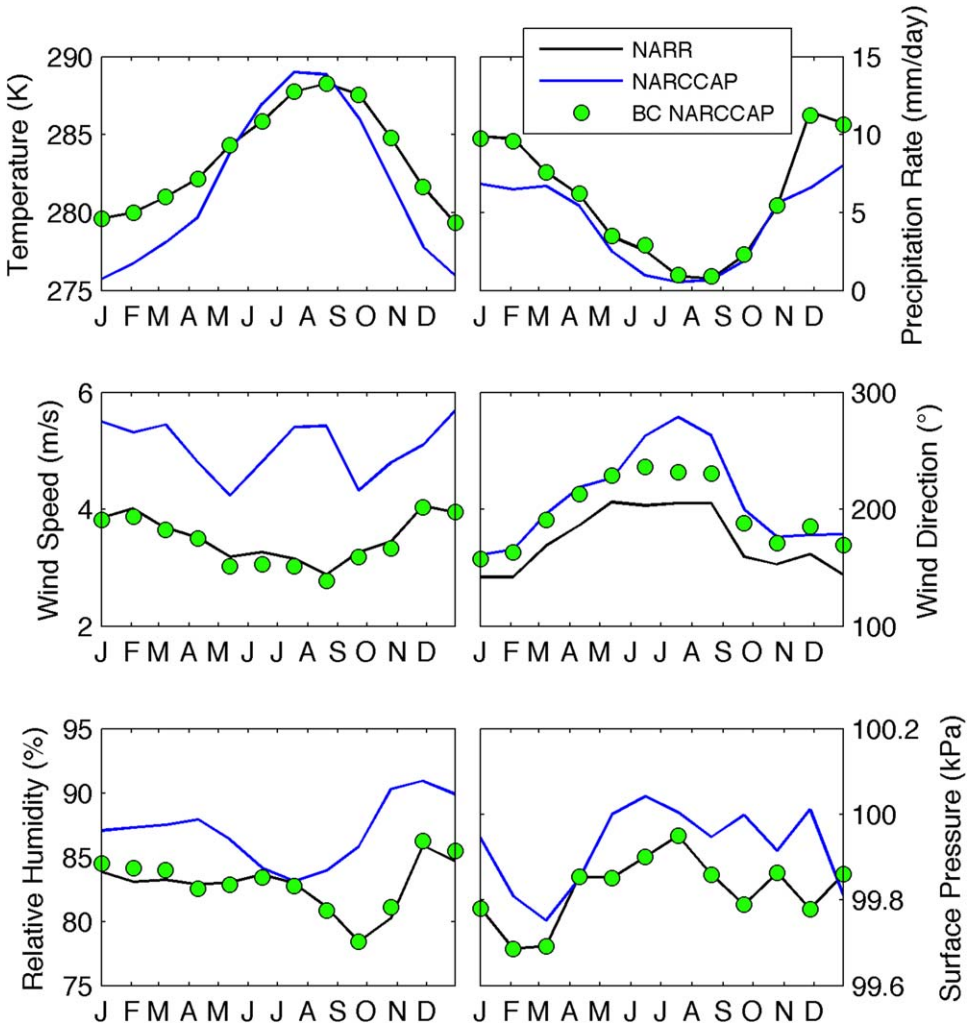

Figure 5. Monthly mean comparisons for historical data sets between NARR, raw NARCCAP, and bias-corrected NARCCAP.

boundary; however, since the spatial rate of change in regional bias is small compared to the spatial rate of change in wave parameters, H_s and T_m from Station #46005, which is further offshore, were used as targets for correction. A Clayton bivariate model was used, assuming Rayleigh and Weibull marginal distributions for H_s and T_m, respectively. The means and variance in observed wave parameters were reproduced in the corrected data through the copula method. Mean wave direction from WW3 was not bias-corrected since directional data were not available from Station #46005 and were unreliably spotty at Station #46029. Seasonal directionality in modeled wave direction was well reproduced however, with waves arriving from the southwest in the winter and from the northwest in the summer.

A comparison of the monthly mean significant wave heights and mean wave periods from the bias-corrected wave data is shown in Figure 7. Average magnitudes for wave heights in the future scenario are generally lower than that of the historical scenario. *Hemer et al.* [2013] found a projected decrease in annual mean significant wave height in a quarter of the global ocean area, including the Eastern North Pacific, especially in the winter season, using a multimodel ensemble. *Graham et al.* [2012] noted a decrease in winter wave heights in their three-model (one of which was CCSM) study of the IPCC A2 scenario. Using a multimodel CMIP5 ensemble, *Wang et al.* [2014] also saw a decrease in wave height magnitudes for the domain when comparing between the late 20th and 21st centuries.

At the time of model simulation, spatially variable open boundary wave forcing for the parallel version of ADCIRC-SWAN had not yet been implemented. However, a comparison of WW3 output at various locations

© 2014. American Geophysical Union. All Rights Reserved.

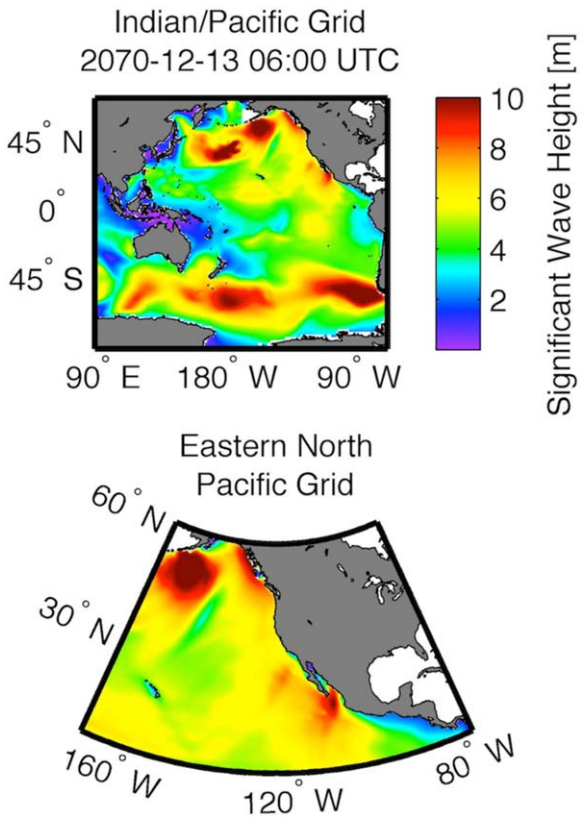

Figure 6. WW3 prediction of significant wave height using the global and eastern North Pacific Ocean grids at 1° by 1.25° and 0.25° by 0.25° spatial resolution, respectively. Data are for 13 December 2070 06:00 UTC.

along the ADCIRC-SWAN open boundary showed there was little variability in offshore wave heights and periods. Therefore, a single wave-forcing file with bulk wave parameters found by integrating the WW3 output wave spectra was prescribed for the ocean boundary.

2.5.2. Open Boundary Forcing-Tides

Tidal amplitudes and phases were extracted from the ENPAC tidal database for seven tidal constituents (M2, S2, N2, K2, K1, O1, and Q1) and prescribed at all open ocean boundary nodes [*Spargo et al*., 2004]. To align the tidal signal with the beginning of the historic and future scenarios, the tide_fac ADCIRC utility program (available at www.adcirc.org) provided nodal factors and equilibrium arguments.

2.5.3. Surface Forcing

NARCCAP wind and surface pressure data were corrected using the quantile mapping procedure with NARR as a target [*Wood et al*., 2004]. Bias-corrected wind velocity components and mean sea level surface pressure values were interpolated onto a regular grid of 0.1° spacing. ADCIRC determined the drag coefficient from the wind speed and calculated the wind stress accordingly. These wind stress values were interpolated to the unstructured mesh and passed to SWAN.

2.5.4. Streamflow Forcing

Historical and future data sets of Tillamook Bay streamflow inputs were obtained by adapting a suite of highly distributed, physically based weather, snowmelt, and runoff-routing models to the Tillamook Bay watershed. SnowModel [*Liston and Elder*, 2006a] is a spatially and temporally distributed meteorological and snowpack modeling system that was used to simulate the runoff generated by liquid precipitation fluxes and snowmelt. SnowModel is composed of several submodels: MicroMet defines the meteorological forcing conditions [*Liston and Elder*, 2006b]; EnBal calculates the surface energy exchanges [*Liston*, 1995]; and SnowPack simulates mass and heat transfer processes, including runoff from liquid precipitation and snowmelt [*Liston and Hall*, 1995]. A key output of SnowModel simulations is grid-cell runoff at each model time step. To relate grid-cell runoff to basin runoff hydrographs, the HydroFlow runoff routing model [*Liston and Mernild*, 2012] is used to route the runoff through the coincident river drainage networks.

The end result of this series of models is a complete runoff hydrograph at all model cells, and by summing the runoff from all coastal cells, or taking any cell of interest (e.g., a stream gaging station), the freshwater discharge for the whole Tillamook Bay watershed or local site of interest was determined. The HydroFlow runoff hydrographs were then compared with observed river discharges, thus providing a validated measure of model-simulated water balances over time scales ranging from individual storms and melt events, to seasonal and annual cycles.

Watershed delineation of the USGS 1/3 arc sec DEM [*Gesch et al*., 2002] of the Tillamook Bay watershed indicated that 95% of the basin is drained by four primary rivers (Miami River, Kilchis River, Wilson River, and Trask River). Of these, long-term stream gauge data were available at three stations located upstream from

© 2014. American Geophysical Union. All Rights Reserved.

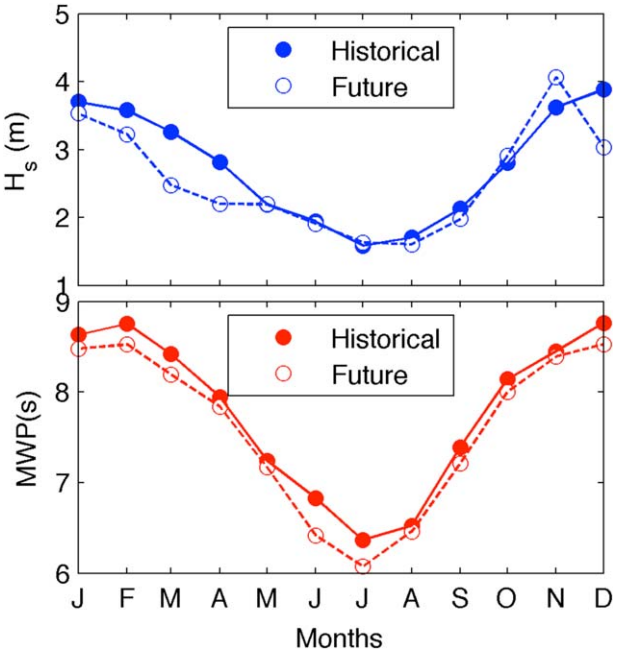

Figure 7. Monthly mean values of significant wave height (H_s) and mean wave period (MWP) for the historical and future scenarios.

the outlets of the Miami, Wilson, and Trask (Figure 1c). Simulated runoff hydrographs were extracted from grid cells located at the three stream gauging stations for validation of the hydrologic model and at the four basin outlets to serve as the freshwater input time series for the Tillamook Bay tidal hydrodynamics model.

To calibrate the model, air temperature, precipitation, relative humidity, and wind speed and direction were extracted from the NARR data set at nine grid points for the period 1 September 1995 to 31 August 1998. The USGS DEM was resampled to a 100 m resolution grid covering a 45 km (north-south) by 60 km (east-west) domain encompassing all of the Tillamook watershed. Vegetation classes for each grid cell were obtained from the National Land Cover Database 2001, v.1.0, resampled to the 100 m model grid and reclassed to match the vegetation classes specified by *Liston and Elder* [2006b].

Figure 8 shows a comparison between the observed and modeled hydrographs for the three gaged watersheds. Nash-Sutcliffe efficiencies (NSE) exceed 0.75 and r^2 values exceed 0.89 for all sites. The NSE is given by

$$NSE = 1 - \frac{\sum_{t=1}^{T} \left(Q_o^t - Q_m^t\right)^2}{\sum_{t=1}^{T} \left(Q_o^t - \overline{Q_o}\right)^2}, \quad (1)$$

where Q_o is an observed value, Q_m is a modeled value, the overbar indicates the temporal mean, and the summation is over all of the values in a time series. An NSE of 1 indicates a perfect match, while a value of 0 indicates that the observed mean is as good of a predictor as the model. The modeled runoff for the Miami and Wilson rivers has a negative bias, while the Trask has a slight positive bias. In general, the simulated runoff does a very good job in capturing both the annual variation in streamflow and the runoff from individual storms.

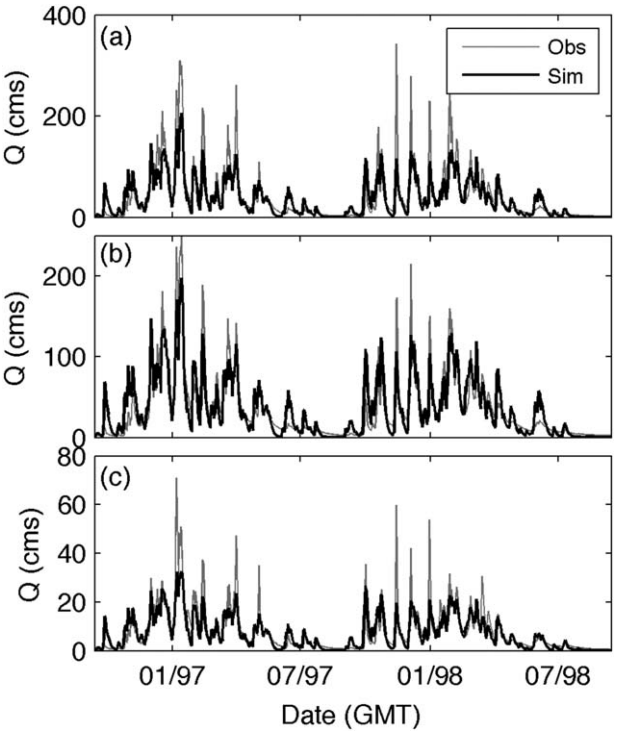

Figure 8. Comparison of observed (Obs) and modeled (Sim) hydrographs at the (a) Wilson, (b) Trask, and (c) Miami Rivers.

With the model calibrated, long-term runs were carried out by extracting bias-corrected NARCCAP data at six grid points for the periods 1 January 1979 to 31 December 1998 and 1 January 2041 to 31 December 2070. The mean annual discharge into Tillamook

© 2014. American Geophysical Union. All Rights Reserved.

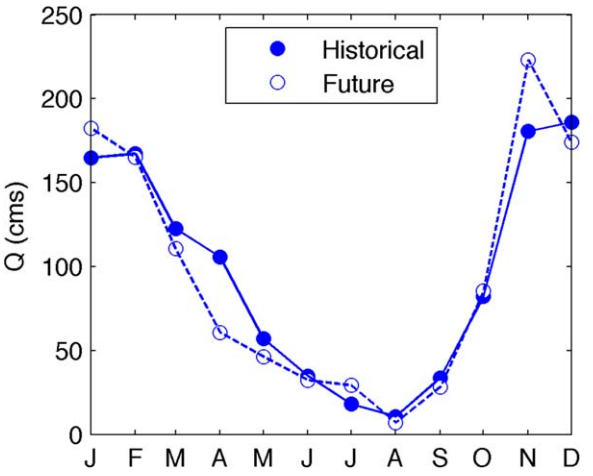

Figure 9. Mean monthly discharges averaged over combined point sources for the historical (1979–1998) and future (2041–2060) scenarios.

Bay (the sum of the four rivers) was 3.02 $km^3\ yr^{-1}$ for the historical run, decreasing slightly to 2.98 $km^3\ yr^{-1}$ for the future run. Figure 9 shows the mean annual hydrograph for the two periods and it is noted that, under the future climate scenario, spring runoff decreases, but winter runoff increases. The combined (over the four rivers) peak flow rate was 780 $m^3\ s^{-1}$ for the historic run and 1120 $m^3\ s^{-1}$ for the future, indicating greater future variability in streamflow.

3. Results

A 1 month run, with tidal forcing only, was conducted in order to verify the model's ability to accurately reproduce the tidal signal. Model output at the location of the Garibaldi tide gage was compared to the observations at that location (Figure 10). The NSE was found to be 0.96, indicating excellent agreement.

Continuous water surface elevation and significant wave height time series were then output at 500 randomly selected nodes within the −2 to 2 m depth range as well as various points at other locations of interest (e.g. jettied inlet, NOAA tide gauge location, open coast). Figure 11 displays the output station locations and the distribution of points across half-meter depth bins and spatial quadrants. The eastern side of the bay contains the bulk of output stations due to the predominance of wetlands and tidal flats. In contrast, shallow-water regions in the western portion are mostly characterized by narrow strips of estuarine beach.

Total water levels are calculated as a linear superposition of the water surface elevation (ζ) and one half the significant wave height (H_s)

$$TWL = \zeta + \frac{1}{2}H_s \tag{2}$$

The water surface elevation output from ADCIRC captures the tidal signal, wind-blown surge and streamflow contributions. Although wave runup has typically been included in total water level calculations within coastal engineering literature [*Holman and Guza*, 1984; *Stockdon et al*., 2006], the empirical formulations in those studies have primarily been developed for open-coast dune-backed beaches, with well-defined beach slopes. The more variable bathymetry of estuaries makes application of those runup formulae speculative and, as a result, the simpler approach of equation (2) is used to capture the additional inundation potential of the waves themselves.

Figure 12 shows representative time series at a single point within the bay for both long-term historical and future scenarios. This particular point lies at 50 cm above MSL for the historic period. As a result, the node is only intermittently wet, resulting in the truncated water elevation signal at low tide. For the future simulation (Figures 12c–12d), water elevations are referenced to the new MSL. In both sets of simulations, annual

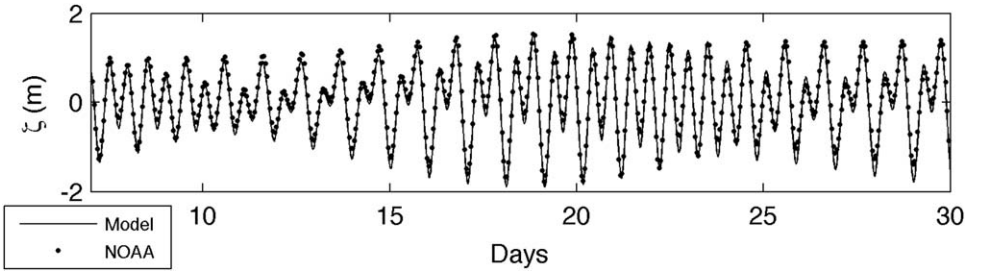

Figure 10. Comparison of modeled and NOAA reported water elevations at the Garibaldi gauge.

© 2014. American Geophysical Union. All Rights Reserved.

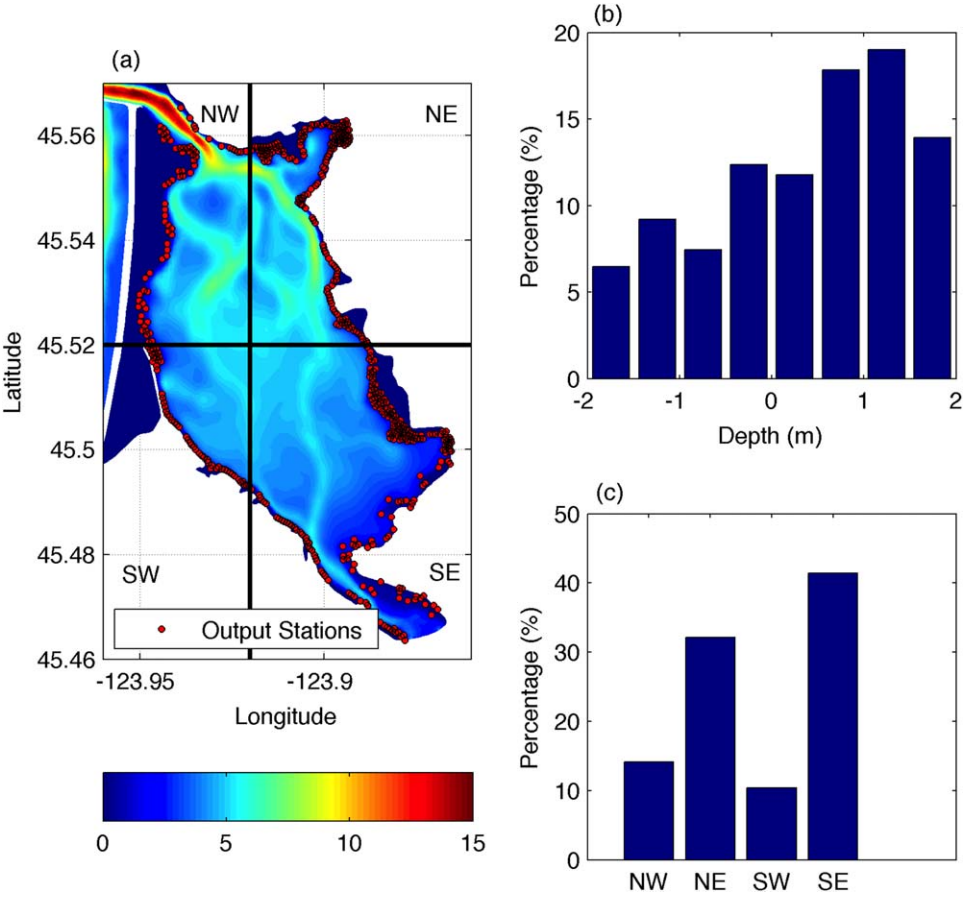

Figure 11. Output station locations (a) in Tillamook Bay; histograms showing (b) the depth distribution; (c) geographic distribution of the stations. Color bar shows bathymetry in meters.

peaks in significant wave height corresponding to the winter season are evident; it is also clear that wave heights are slightly larger at this location in the future simulation. A close-up of the future time series (Figures 12e–12f) shows the growth and decay of the significant wave height over short-term durations (e.g. hours, days) more clearly.

Cumulative distribution functions (CDFs) can be generated from these long-term time series, either seasonally or using the entire year. Since the presence of strong winter storms and relatively mild summers on the Oregon coast represent two distinct climes, CDFs are calculated seasonally to analyze the relative difference, if any, between the two when comparing the historic and future scenarios. Figure 13 shows the CDFs at several representative points inside and outside the bay, for both summer and winter periods and for both the historic and future simulations. In this figure, the water elevations for both time periods are referenced to the historic MSL. Therefore, the shifts between historic and future plots represent a combination of SLR and other hydrodynamic changes.

Geographic location and local effects have a large impact on the relative translation observed between the winter and summer seasons. The open coast locations (Figures 13a and 13e) show the largest differences between summer and winter, and the largest TWL values overall. These results are due primarily to the presence of large waves offshore in the winter season. These waves are unable to penetrate very far into Tillamook Bay [*Cheng et al.*, 2014] resulting in an ocean-to-bay gradient in the differences between winter and summer CDFs. Figure 13c shows the conditions in the jettied inlet, where some wave penetration is found. Figure 13b shows the conditions at the Garibaldi tide gage (further in the bay) and the winter/summer distinction is now quite small. It is even smaller in the south bay (Figure 13d), which is due to local wind generation in the bay itself. Prevailing winds during the winter blow from the south, generating local seas up to 1 m in wave height in the northern reaches of the bay. These local seas provide the slight seasonal differences found at the Garibaldi location, but absent in the south bay.

© 2014. American Geophysical Union. All Rights Reserved.

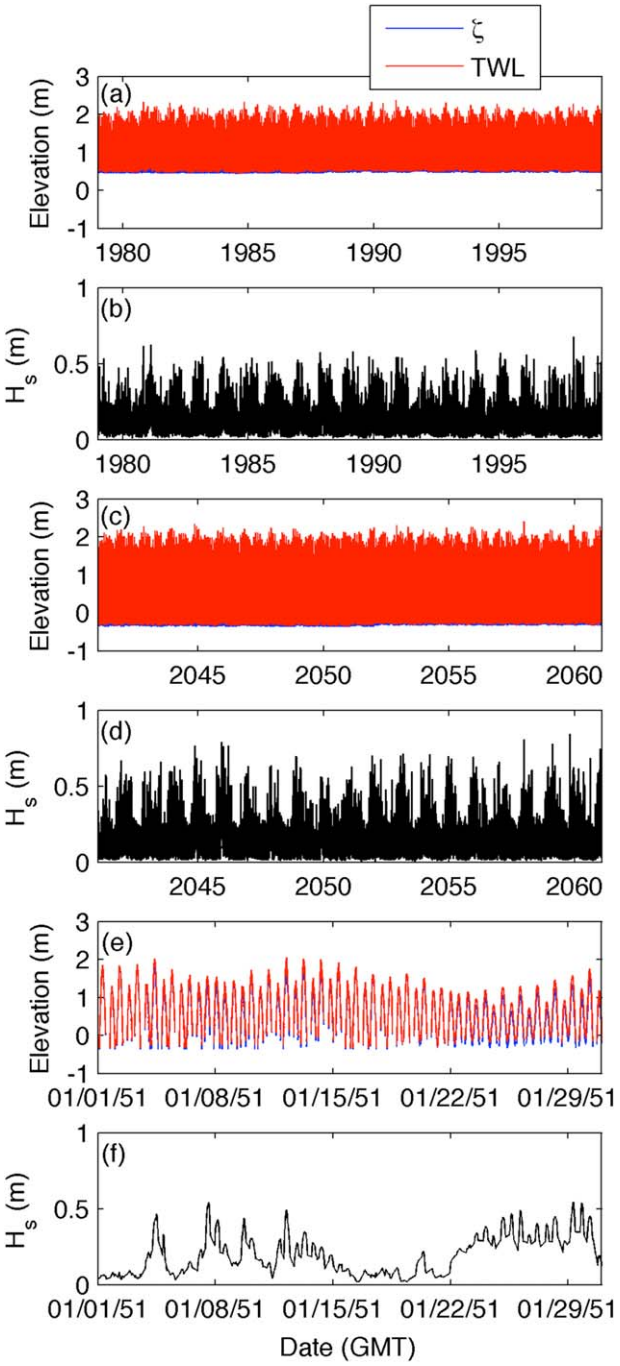

Figure 12. Time series of ζ, TWL, and H_s for (a, b) the historic period, (c, d) the future simulation, and (e, f) a 1 month zoomed in view of the future simulation.

At most of the locations, the climate change signal appears fairly weak, with the future CDFs appearing to be simply translated 80 cm (the amount of SLR assumed). Figure 13f shows the CDFs at a shallow point in the bay and is a clear exception. Located at an elevation of 50 cm above the historic MSL, the point has a historic CDF that is "truncated" at the lower end, due to the intermittent wetting and drying at that location. The future CDF shows the increase in elevation due to the SLR and indicates that the lower limit is again controlled by drying of the node. The effect of SLR on TWL values therefore depends both on the elevation of the point and its spatial proximity to various physical processes such as locally generated waves, river inputs, etc.

TWLs corresponding to various return periods were calculated for both scenarios for three depth bins, $-1\ \text{m} \leq h < 0\ \text{m}$, $0\ \text{m} \leq h < 1\ \text{m}$, and $1\ \text{m} \leq h < 2\ \text{m}$. These results are shown in Figure 14 and are more revealing, in terms of any climate-change-induced impact. First, note that, for comparison, the NOAA extreme water levels from South Beach (Station #9435380) are included in all panels. These values are not provided for the Garibaldi station. Next, in this figure, as with Figure 12, the TWL values are referenced to the MSL corresponding to the time period in question, so any change in TWL is above and beyond the SLR component. Recall that in ADCIRC depths are positive. There are several interesting observations to be made. First, for all depth bins, extreme TWLs are greater in the northern bay than in the southern. This is primarily due to a combination of wind-blown surge (south to north) and locally generated seas during winter storms. Second, the difference between TWLs in the north and south is greater in deeper water, with approximately 40 cm difference at the 20 year return period in the deepest bin. The smaller differences observed in the shallower bins is due to the damping effects of shallow water and wetting and drying. For example, locally generated seas generated by strong south to north winds in the winter will break as they propagate into the very shallow reaches of the northern bay. Therefore, their contributions to TWLs diminish. Finally, the climate change signal (above and beyond the SLR change) is more obvious than it was in Figure 13. It is observed that shallow areas in

© 2014. American Geophysical Union. All Rights Reserved.

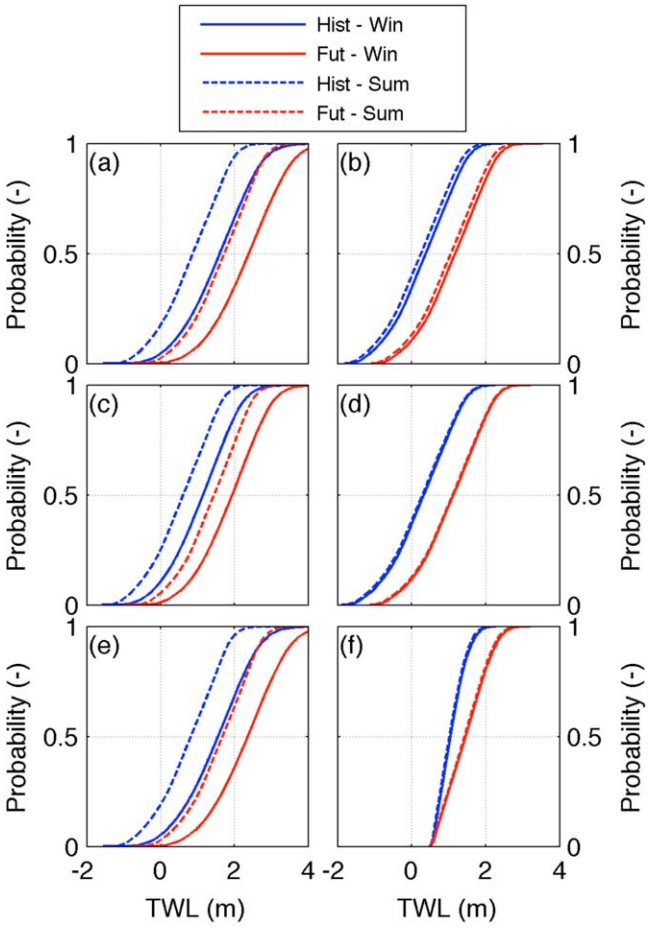

Figure 13. Historic (blue) and future (red) CDFs by season (winter-solid, summer-dashed) for (a) open coast at h = 20 m contour, (b) NOAA tide gauge location, (c) jettied inlet, (d) southern Tillamook Bay, (e) open coast at h = 10 m contour, and (f) shallow-water point within bay.

the northern bay experience the greatest change, with increases in the 20 year value of about 15–20 cm, on top of the 80 cm SLR component.

4. Discussion

The statistics related to TWLs in Tillamook Bay can be assessed from several perspectives: seasonal, geographical, and in relation to the time duration of major storms. A seasonal signal is present in both the historical and future scenario TWLs, with winter water levels consistently higher than those of summer (Figures 13 and 14). The relative strength of this signal depends on the local environment. As Figure 13 shows, seasonal differences in TWLs decrease sharply from open coast to estuarine environments. The reduction in magnitudes can be attributed to the limited wind fetch available for wave growth inside the bay and dissipation of offshore wave heights through the bay entrance. Sustained winds and gusts have much larger distances, on the order of hundreds or thousands of kilometers, over the Pacific Ocean to create large storm wave heights. In contrast, the length of the longest fetch over Tillamook Bay is about 10 km. Therefore, the contribution that significant wave height has toward TWLs in the bay in the winter is effectively capped. Summer winds are typically directed from the NW but are of lower magnitude.

This should not be interpreted to mean that offshore waves do not impact inner estuarine waters, however. *Cheng et al.* [2014] recently completed a study of extreme storms in Tillamook Bay and one of the major findings was that offshore waves are the primary driver of nontidal residuals (NTRs) in the Bay. Radiation stress gradients setup by the breaking of large (10 m) offshore waves can lead to NTRs between 1 and 2 m in Tillamook Bay and other PNW estuaries. It is well known that direct storm surge effects are weak on the West Coast, compared to the East and Gulf Coasts, so this finding points to the major flooding mechanism for small, West Coast estuaries.

An assessment of TWL by quadrants (Figure 11) in the bay yields additional perspective on the spatial variation of water levels. To illuminate this, the 99th percentile values of TWL were calculated for the quadrants and for the deepest depth bin and are summarized in Table 1 for the historical and future scenarios. The proximity of the SE quadrant to the Wilson and Trask River watersheds, which contribute the bulk of the gauged streamflow, results in the SE quadrant consistently having (summer and winter; historic and future) the highest 99th percentile value. The NE quadrant is consistently second highest, due in parts to the proximity to the Miami River and to exposure to locally generated waves and surge in the bay. The SW has the lowest values since it is not near any river discharge, has limited exposure to waves, and is on the windward side (reduction in water surface elevation) of surge within the bay.

The work of *Cheng et al.* [2014], through a systematic study of the individual processes controlling NTRs, corroborates that streamflow has a noticeable effect on water levels throughout the bay. However, even for

© 2014. American Geophysical Union. All Rights Reserved.

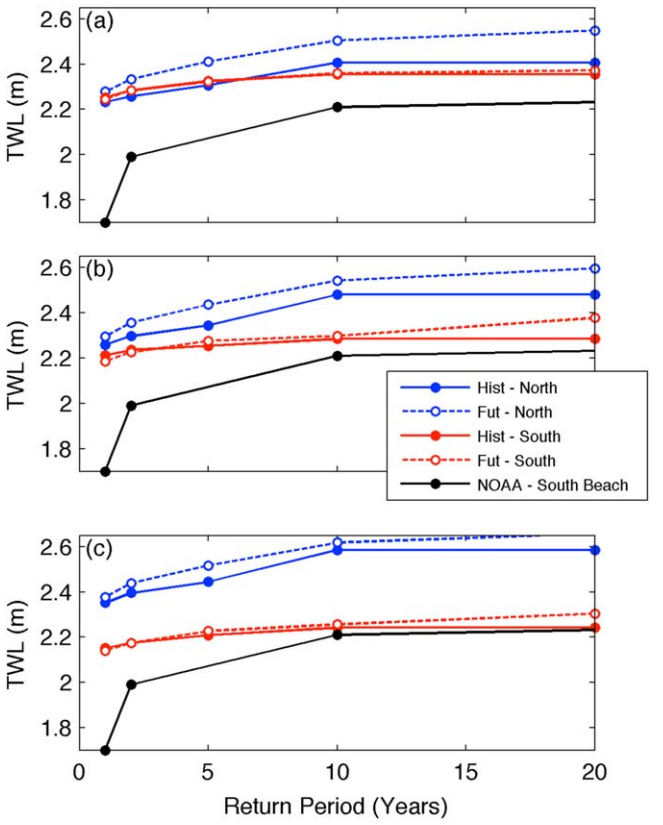

Figure 14. Total water levels associated with varying return periods for points in northern (blue) and southern (red) halves of Tillamook Bay. Solid lines correspond to the historic simulation and dashed lines the future simulation. Curves were calculated for depth bins (a) $-1\ \text{m} \leq h < 0\ \text{m}$, (b) $0\ \text{m} \leq h < 1\ \text{m}$, and (c) $1\ \text{m} \leq h < 2\ \text{m}$.

extreme discharge events (the 2007 storm studied in that paper produced approximately a 20 year flow), the effect is secondary compared to that of offshore wave breaking.

The spatial variability observed in the CDFs (Figure 13) and, more notably, in the extreme values (Figure 14) is of value in providing improved flood products (maps, etc.) to estuarine communities. FEMA mapping products have historically focused on riverine and open coastal environments, with inadequate attention given to the estuarine intersection. As an example, the Flood Insurance Study (FIS) [*FEMA*, 2002] for Tillamook describes HEC-2 hydraulic analysis that was used to compute water levels in the rivers contributing to Tillamook Bay, but that methodology is clearly not applicable to regions influenced by tides and waves. Estimates of TWLs on the open coast, on the other hand, are primarily supported by data from long-term tide gauges. The original FEMA maps from the 1970s and 1980s relied on the distant Crescent City, CA gauge (and interpolation).

Revisions to FEMA mapping products are presently underway and use methods with varying degrees of modification from the past. For riverine regions, the original water levels are still being used, but are being laid over vastly improved (LIDAR additions, etc.) DEMs, producing improved estimates of inundated regions. Additional improvements will be obtained when investments are made in new hydraulic modeling. For the open coast regions, *Allan et al*. [2012] provide a valuable template for improved estimates. They compute total water levels by linearly superposing tides (using a network of tide gauges rather than solely the Crescent City gauge) waves (from SWAN modeling) and runup.

Neither of the two approaches above, however, will accurately predict extreme water levels in estuarine environments, where hydrodynamic forcing is sourced both by the ocean and by rivers. Consideration of tides alone will significantly underestimate water levels in these regions, pointing to a need for new methods such as the one presented here.

5. Conclusions

A long-term climatological study of estuarine wave and water elevation conditions for a historical and future scenario was carried out for Tillamook Bay using coupled ADCIRC-SWAN. This paper represents the first attempt to directly model climate change impacts on the hydrodynamics of an estuary over multiple multidecade periods. The methodology is computationally intensive, but provides complete spatiotemporal coverage of water elevations and wave conditions in the bay. This allows for a variety of statistical analyses to be performed, such as determining the TWLs for various return periods, and the exceedance probabilities of various TWLs.

© 2014. American Geophysical Union. All Rights Reserved.

Table 1. The 99th Percentile TWL Values Within Tillamook Bay for Historical (1979–1998) and Future (2041–2060) Scenarios[a]

	Historical		Future	
Quadrant	Winter	Summer	Winter	Summer
Northwest				
1 m $\leq$ h $<$ 2 m	1.94	1.88	2.70	2.63
Northeast				
1 m $\leq$ h $<$ 2 m	1.98	1.92	2.89	2.83
Southwest				
1 m $\leq$ h $<$ 2 m	1.91	1.85	2.74	2.68
Southeast				
1 m $\leq$ h $<$ 2 m	2.02	1.95	2.94	2.89

[a]Values are referenced to the MSL of the historic period.

Results show that aggregate climate impacts on relative sea level, wind and wave climate, and streamflow result in slightly enhanced total water levels everywhere in Tillamook Bay, although the degree of increase is highly dependent on location, i.e., proximity to contributing processes such as surge from offshore wave breaking or river flow. Local wind sheltering effects from topography also play a role in the magnitude of TWLs. Latitudinally speaking, the southern portion of the bay experiences lower TWLs than the northern bay in both the baseline and projected future model runs. The northern portion of the bay also sees a larger difference between historic and future TWLs associated with longer return periods.

There are several important limitations of the present study. First, only a single GCM/RCM model pairing was used due, in part, to computational expense. Approximately 2000 core-hours were required to simulate 1 year. Two multidecade simulations (one historic, one future) require on the order of 100,000 core-hours. It is clearly desirable to conduct an ensemble of runs forced with different climate models. This will help to bracket the anticipated changes observed in TWLs. An ensemble of 5–10 GCM/RCM pairings will therefore cost 0.5–1.0 M core-hours. This considerable cost could be reduced somewhat by modeling only October–April, which is when the vast majority of large storm events occur in the PNW.

An alternate path forward, however, is an approach in which individual physical processes are modeled using simpler tools and then summed together. For example, local wind surge in Tillamook Bay could be estimated using the classic one-dimensional force balance on the water column, requiring only fetch, depth, and wind speed/direction. Setup in the bay itself could be estimated from knowledge of the offshore wave height. In this fashion PDFs of meteorological and wave conditions could be efficiently transformed into PDFs of estuarine water levels. The work of *Cheng et al.* [2014] essentially prioritizes processes in estuaries and this information should be used to investigate the feasibility of a reduced modeling effort. The complete time series results of the present study can act as the baseline by which a reduced modeling effort's success can be measured.

Another limitation of the present study is the use of a barotropic circulation model. The present ADCIRC-SWAN model pairing captures the physical processes of waves, tides, streamflow, wave breaking-induced setup, and direct storm surge. Absent from the portfolio of physical processes are effects related to water temperature, baroclinic circulations, and upwelling, among others. Many of these processes have a noticeable effect on water levels in the Pacific Northwest. With increasing model efficiency and computational speed, it is expected that similar modeling efforts that tightly couple baroclinic circulation models (ADCIRC 3D, FVCOM, ROMS, or other) with wave models (SWAN or other) will be possible. This will not only provide a more accurate picture of climate change impacts on water elevations, but will be able to quantify climate change impacts on water column properties.

A final limitation is the study of only one estuary, characterized by its particular balance of ocean and terrestrial forcing. Similar studies in estuaries with markedly different physical balances (say, with a much larger watershed to estuary area ratio) should reveal different patterns of response to changes in offshore wave and streamflow conditions.

In summary, however, the present study has successfully illustrated a physically based, deterministic process for evaluating climate change impacts on estuary water levels. This process, and the results, should be of use to efforts to map out future flooding hazards in coastal waterways.

Acknowledgments

This work was funded in part by the Oregon Sea Grant. The authors are grateful for assistance with coupled ADCSWAN from Casey Dietrich (North Carolina State University) and Marcel Ziljema (Technical University of Delft, Netherlands). This project used the Extreme Science and Engineering Discovery Environment (XSEDE), which is supported by National Science Foundation grant number OCI-1053575. In compliance with AGU's data policy, we point out that the necessary data for this study are all open source and can be found as directed in the various citations related to the input data streams.

References

Abatzoglou, J. T., and T. J. Brown (2011), A comparison of statistical downscaling methods suited for wildfire applications, *Int. J. Climatol.*, *32*(5), pp. 772–780, doi:10.1002/joc.2312.

Allan, J. C., and P. D. Komar (2000), Are ocean wave heights increasing in the eastern North Pacific?, *Eos Trans. AGU*, *47*, 561–567.

Allan, J. C., and P. D. Komar (2001), Wave climate change and coastal erosion in the US Pacific Northwest, in *Proceedings of the 4th International Symposium on Ocean Wave Measurement and Analysis*, edited by B. L. Edge and J. M. Hemsley, pp. 680–690, San Francisco, Calif.

© 2014. American Geophysical Union. All Rights Reserved.

Allan, J. C., and P. D. Komar (2006), Climate controls on US West Coast erosion processes, *J. Coastal Res.*, *22*(3), 511–529.
Allan, J. D., P. Ruggiero, and J. T. Roberts (2012), Coastal flood insurance study, Coos County, Oregon, *Spec. Pap. 44*, 127 p., Oreg. Dep. of Geol. and Miner. Ind., Portland, OR.
Barbier, E. B., S. D. Hacker, C. Kennedy, E. W. Koch, A. C. Stier, and B. R. Silliman (2011), The value of estuarine and coastal ecosystem services, *Ecol. Monogr.*, *81*(2), 169–193.
Barnard, P. L., M. van Ormondt, L. H. Erikson, J. Eshleman, C. Hapke, P. Ruggiero, P. N. Adams, and A. C. Foxgrover (2014), Development of the Coastal Storm Modeling System (CoSMoS) for predicting the impact of storms on high-energy, active-margin coasts, *Nat. Hazards*, *74*(2), 1095–1125.
Boé, J., L. Terray, F. Habets, and E. Martin (2007), Statistical and dynamical downscaling of the Seine basin climate for hydro-meteorological studies, *Int. J. Climatol.*, *27*(12), 1643–1655, doi:10.1002/joc.1602.
Bolch, T., B. Menounos, and R. Wheate (2010), Landsat-based inventory of glaciers in western Canada, 1985–2005, *Remote Sens. Environ.*, *114*(1), 127–137.
Booij, N., R. Ris, and L. Holthuijsen (1999), A third-generation wave model for coastal regions: 1. Model description and validation, *J. Geophys. Res.*, *104*(C4), 7649–7666.
Burger, G., J. Schulla, and A. Werner (2011), Estimates of future flow, including extremes, of the Columbia River headwaters, *Water Resour. Res.*, *47*, W10520, doi:10.1029/2010WR009716.
Carignan, K. S., L. A. Taylor, B. W. Eakins, R. R. Warnken, T. Sazonova, and D. C. Schoolcraft (2009a), *Digital Elevation Model of Garibaldi, Oregon: Procedures, Data Sources and Analysis*, Natl. Ocean. and Atmos. Admin., Boulder, Colo.
Carignan, K. S., L. A. Taylor, B. W. Eakins, R. R. Warnken, E. Lim, and P. R. Medley (2009b), *Digital Elevation Model of Central Oregon Coast: Procedures, Data Sources and Analysis*, Natl. Ocean. and Atmos. Admin., Boulder, Colo.
Charles, E., D. Idier, P. Delecluse, M. Déqué, and G. Le Cozannet (2012), Climate change impact on waves in the Bay of Biscay, France, *Ocean Dyn.*, *62*(6), 831–848, doi:10.1007/s10236-012-0534-8.
Chen, J., F. P. Brissette, D. Chaumont, and M. Braun (2013), Finding appropriate bias correction methods in downscaling precipitation for hydrologic impact studies over North America, *Water Resour. Res.*, *49*, 4187–4205, doi:10.1002/wrcr.20331.
Cheng, T., D. Hill, and W. Read (2014), The contribution to storm tides in Pacific Northwest estuaries: Tillamook Bay, Oregon and the December 2007 storm, *J. Coastal Res.* [Available at doi:10.2112/JCOASTRES-D-14-00120.1.]
Christensen, J. H., F. Boberg, O. B. Christensen, and P. Lucas-Picher (2008), On the need for bias correction of regional climate change projections of temperature and precipitation, *Geophys. Res. Lett.*, *35*, L20709, doi:10.1029/2008GL035694.
Corbella, S., and D. Stretch (2012), Predicting coastal erosion trends using non-stationary statistics and process-based models, *Coastal Eng.*, *70*, 40–49.
De Waal, D., and P. van Gelder (2005), Modelling of extreme wave heights and periods through copulas, *Extremes*, *8*(4), 345–356.
Dietrich, J. C., M. Zijlema, J. J. Westerink, L. H. Holthuijsen, C. Dawson, R. A. Luettich, R. E. Jensen, J. M. Smith, G. S. Stelling, and G. W. Stone (2011a), Modeling hurricane waves and storm surge using integrally-coupled, scalable computations, *Coastal Eng.*, *58*(1), 45–65, doi:10.1016/j.coastaleng.2010.08.001.
Dietrich, J. C., S. Tanaka, J. J. Westerink, C. N. Dawson, R. A. Luettich, M. Zijlema, L. H. Holthuijsen, J. M. Smith, L. G. Westerink, and H. J. Westerink (2012a), Performance of the unstructured-mesh, SWAN+ADCIRC model in computing hurricane waves and surge, *J. Sci. Comput.*, doi:10.1007/s10915-011-9555-6.
Dietrich, J. C., M. Zijlema, P.-E. Allier, L. H. Holthuijsen, N. Booij, J. D. Meixner, J. K. Proft, C. N. Dawson, C. J. Bender, A. Naimaster, J. M. Smith, and J. J. Westerink (2012b), Limiters for spectral propagation velocities in SWAN, *Ocean Modell.*, *70*, 85–102.
Ehret, U., E. Zehe, V. Wulfmeyer, K. Warrach-Sagi, and J. Liebert (2012), Should we apply bias correction to global and regional climate model data?, *Hydrol. Earth Syst. Sci.*, *16*(9), 3391–3404, doi:10.5194/hess-16-3391-2012.
Elguindi, N., and A. Grundstein (2013), An integrated approach to assessing 21st century climate change over the contiguous U.S. using the NARCCAP RCM output, *Clim. Change*, *117*(4), 809–827, doi:10.1007/s10584-012-0552-z.
FEMA (2002), *Flood Insurance Study, City of Tillamook, Oregon, Tillamook County*, 43 pp., Washington, D. C.
Ferreira, J. A., and C. G. Soares (2002), Modelling bivariate distributions of significant wave height and mean wave period, *Appl. Ocean Res.*, *24*(1), 31–45, doi:10.1016/S0141-1187(02)00006-8.
Frei, C., R. Schöll, S. Fukutome, J. Schmidli, and P. L. Vidale (2006), Future change of precipitation extremes in Europe: Intercomparison of scenarios from regional climate models, *J. Geophys. Res.*, *111*, D06105, doi:10.1029/2005JD005965.
Gallien, T. W., J. E. Schubert, and B. F. Sanders (2011), Predicting tidal flooding of urbanized embayments: A modeling framework and data requirements, *Coastal Eng.*, *58*, 567–577.
Gesch, D., M. Oimoen, S. Greenlee, C. Nelson, M. Steuck, and D. Tyler (2002), The national elevation dataset, *Photogramm. Eng. Remote Sens.*, *68*(1), 5–11.
Graham, N. E., and H. Diaz (2001), Evidence for intensification of North Pacific winter cyclones since 1948, *Bull. Am. Meteorol. Soc.*, *82*, 1869–1893.
Graham, N. E., D. R. Cayan, P. D. Bromirski, and R. E. Flick (2012), Multi-model projections of twenty-first century North Pacific winter wave climate under the IPCC A2 scenario, *Clim. Dyn.*, *40*, 1335–1360, doi:10.1007/s00382-012-1435-8.
Gray, W. (1982), Some inadequacies of finite element models as simulators of two-dimensional circulation, *Adv. Water Resour.*, *5*(3), 171–177.
Haerter, J., S. Hagemann, C. Moseley, and C. Piani (2011), Climate model bias correction and the role of timescales, *Hydrol. Earth Syst. Sci.*, *15*(3), 1065–1079, doi:10.5194/hess-15-1065-2011.
Hamlet, A., P. Mote, M. Clark, and D. Lettenmaier (2005), Effects of temperature and precipitation variability on snowpack trends in the western United States, *J. Clim.*, *18*(21), 4545–4561.
Hanson, J. L., B. A. Tracy, H. L. Tolman, and R. D. Scott (2009), Pacific hindcast performance of three numerical wave models, *J. Atmos. Ocean. Technol.*, *26*(8), 1614–1633.
Hasselmann, S., K. Hasselmann, J. H. Allender, and T. P. Barnett (1985), Computations and parameterizations of the nonlinear energy transfer in a gravity-wave spectrum. Part II: Parameterizations of the nonlinear energy transfer for application in wave models, *J. Phys. Oceanogr.*, *15*, 1378–1391.
Hemer, M. A., Y. Fan, N. Mori, A. Semedo, and X. L. Wang (2013), Projected changes in wave climate from a multi-model ensemble, *Nat. Clim. Change*, *3*(5), 471–476, doi:10.1038/nclimate1791.
Holman, R. A., and R. T. Guza (1984), Measuring run-up on a natural beach, *Coastal Eng.*, *8*, 129–140.
IPCC (2007), Climate Change 2007: The physical science basis, in *Contribution of Working Group I to the Fourth Assessment Report of the Intergovernmental Panel on Climate Change*, edited by S. Solomon et al., 996 pp., Cambridge Univ. Press, Cambridge, U. K.

© 2014. American Geophysical Union. All Rights Reserved.

Kuang, C., W. Chen, J. Gu, D. Z. Zhu, L. He, and H. Huang (2014), Numerical assessment of the impacts of potential future sea-level rise on hydrodynamics of the Yangtze River Estuary, China, *J. Coastal Res.*, *295*, 586–597.
Leung, L. R., Y. Qian, X. Bian, W. M. Washington, J. Han, and J. O. Roads (2004), Mid-century ensemble regional climate change scenarios for the western United States, *Clim. Change*, *62*(1), 75–113, doi:10.1023/B:CLIM.0000013692.50640.55.
Li, H., J. Sheffield, and E. Wood (2010), Bias correction of monthly precipitation and temperature fields from intergovernmental panel on climate change AR4 models using equidistant quantile matching, *J. Geophys. Res.*, *115*, D10101, doi:10.1029/2009JD012882.
Liston, G. E. (1995), Local advection of momentum, heat, and moisture during the melt of patchy snow covers, *J. Appl. Meteorol.*, *34*, 1705–1715.
Liston, G. E., and K. Elder (2006a), A distributed snow-evolution modeling system (SnowModel), *J. Hydrometeorol.*, *7*(6), 1259–1276.
Liston, G. E., and K. Elder (2006b), A meteorological distribution system for high-resolution terrestrial modeling (MicroMet), *J. Hydrometeorol.*, *7*(2), 217–234.
Liston, G. E., and D. K. Hall (1995), An energy-balance model of lake-ice evolution, *J. Glaciol.*, *41*(138), 373–382.
Liston, G. E., and S. H. Mernild (2012), Greenland freshwater runoff. Part I: A runoff routing model for glaciated and nonglaciated landscapes (HydroFlow), *J. Clim.*, *25*, 5997–6014.
Luettich, R. A., and J. J. Westerink (1991), A solution for the vertical variation of stress, rather than velocity, in a three-dimensional circulation model, *Int. J. Numer. Methods Fluids*, *12*(10), 911–928.
Luettich, R. A., and J. J. Westerink (2004), Formulation and numerical implementation of the 2D/3D ADCIRC finite element model version 44.XX, technical report, 74 pp.
Mathisen, J., and E. Bitnergregersen (1990), Joint distributions for significant wave height and wave zero-up-crossing period, *Appl. Ocean Res.*, *12*(2), 93–103.
Maurer, E., and H. Hidalgo (2008), Utility of daily vs. monthly large-scale climate data: An intercomparison of two statistical downscaling methods, *Hydrol. Earth Syst. Sci.*, *12*(2), 551–563, doi:10.5194/hess-12-551-2008.
Mearns, L. O., W. J. Gutowski, R. Jones, L.-Y. Leung, S. McGinnis, A. M. B. Nunes, and Y. Qian (2009), A regional climate change assessment program for North America, *Eos Trans. AGU*, *90*(36), 311–312.
Mearns, L. O., et al. (2013), Climate change projections of the North American regional climate change assessment program (NARCCAP), *Clim. Change*, *120*(4), 965–975, doi:10.1007/s10584-013-0831-3.
Mesinger, F., et al. (2006), North American regional reanalysis: A long-term, consistent, high-resolution climate dataset for the North American domain, as a major improvement upon the earlier global reanalysis datasets in both resolution and accuracy, *Bull. Am. Meteorol. Soc.*, *87*(3), 343–360.
Miller, N. L., J. Kim, R. K. Hartman, and J. Farrara (1999), Downscaled climate and streamflow study of the southwestern United States, *J. Am. Water Resour. Assoc.*, *35*(6), 1525–1537, doi:10.1111/j.1752-1688.1999.tb04235.x.
Mote, P. W., and E. P. Salathé, Jr. (2010), Future climate in the Pacific Northwest, *Clim. Change*, *102*(1), 29–50, doi:10.1007/s10584-010-9848-z.
Myrhaug, D., and E. H. Hansen (1997), Long-term distribution of seabed shear stresses beneath random waves, *Coastal Eng.*, *31*(1), 327–337.
Olabarrieta, M., J. Warner, and N. Kumar (2011), Wave-current interaction in Willapa Bay, *J. Geophys. Res.*, *116*, C12014, doi:10.1029/2011JC007387.
Panofsky, H. A., and G. W. Brier (1958), *Some Applications of Statistics to Meteorology*, Pa. State Univ. Press, University Park.
Pryor, S., J. T. Schoof, and R. Barthelmie (2006), Winds of change?: Projections of near-surface winds under climate change scenarios, *Geophys. Res. Lett.*, *33*, L11702, doi:10.1029/2006GL026000.
Pryor, S. C., R. J. Barthelmie, D. T. Young, E. S. Takle, R. W. Arritt, D. Flory, W. J. Gutowski Jr., A. Nunes, and J. Roads (2009), Wind speed trends over the contiguous United States, *J. Geophys. Res.*, *114*, D14105, doi:10.1029/2008JD011416.
Rahmstorf, S., G. Foster, and A. Cazenave (2012), Comparing climate projections to observations up to 2011, *Environ. Res. Lett.*, *7*(4), doi:10.1088/1748-9326/7/4/044035.
Repko, A., P. H. A. J. M. Van Gelder, H. G. Voortman, and J. K. Vrijling (2004), Bivariate description of offshore wave conditions with physics-based extreme value statistics, *Appl. Ocean Res.*, *26*(3), 162–170.
Resio, D. T., S. M. Bratos, and E. F. Thompson (2008), Meteorology and wave climate, in *Coastal Engineering Manual. Part II: Hydrodynamics*, edited by L. Vincent and Z. Demirbilek, Army Corps of Eng., Washington, D. C.
Ris, R., L. Holthuijsen, and N. Booij (1999), A third-generation wave model for coastal regions: 2. Verification, *J. Geophys. Res.*, *104*(C4), 7667–7681.
Rogers, W. E., P. A. Hwang, and D. W. Wang (2003), Investigation of wave growth and decay in the SWAN model: Three regional-scale applications, *J. Phys. Oceanogr.*, *33*(2), 366–389.
Ruggiero, P., P. Komar, and J. Allan (2010), Increasing wave heights and extreme value projections: The wave climate of the US Pacific Northwest, *Coastal Eng.*, *57*(5), 539–552, doi:10.1016/j.coastaleng.2009.12.005.
Schiefer, E., B. Menounos, and R. Wheate (2007), Recent volume loss of British Columbian glaciers, Canada, *Geophys. Res. Lett.*, *34*, L16503, doi:10.1029/2007GL030780.
Seymour, R. J. (2011), Evidence for changes to the Northeast Pacific wave climate, *J. Coastal Res.*, *27*(1), 194–201, doi:10.2112/JCOASTRES-D-09-00149.1.
Sklar, M. (1959), *Fonctions de répartition à n dimensions et leurs marges*, Université Paris 8, Paris, France.
Solomon, S., et al. (2007), Climate Change 2007: The physical science basis, in *Contribution of Working Group I to the Fourth Assessment Report of the Intergovernmental Panel on Climate Change*, edited by S. Solomon, et al., 996 pp., Cambridge Univ. Press, N. Y.
Spargo, E., J. Westerink, R. Luettich, and D. Mark (2004), ENPAC 2003: A tidal constituent database for eastern North Pacific Ocean, *ERDC/CHL TR-04–12*, US Army Corps of Eng., Washington, D. C.
Stockdon, H. F., R. A. Holman, P. A. Howd, and A. H. Sallenger (2006), Empirical parameterization of setup, swash, and runup, *Coastal Eng.*, *53*(7), 573–588.
Tolman, H. L. (2002a), Alleviating the garden sprinkler effect in wind wave models, *Ocean Modell.*, *4*, 269–289.
Tolman, H. L. (2002b), Validation of WAVEWATCH III version 1.15 for a global domain, *NOAA/NWS/NCEP/OMB 213*, p. 33, Washington, D. C.
Tolman, H. L., and D. Chalikov (1996), Source terms in a third-generation wind wave model, *J. Phys. Oceanogr.*, *26*(11), 2497–2518.
US Army Corp of Engineers Joint Airborne Lidar Bathymetry Technical Center of Expertise (2012), *2010–2011 US Army Corps of Engineers (USACE) Joint Airborne Lidar Bathymetry Technical Center of Expertise (JALBTCX) Topobathy Lidar*, Oregon, Washington, D. C.
Vermeer, M., and S. Rahmstorf (2009), Global sea level linked to global temperature, *Proc. Natl. Acad. Sci. U. S. A.*, *106*(51), 21,527–21,532.
Wang, X. L., Y. Feng, and V. R. Swail (2014), Changes in global ocean wave heights as projected using multimodel CMIP5 simulations, *Geophys. Res. Lett.*, *41*, 1026–1034, doi:10.1002/2013GL058650.

© 2014. American Geophysical Union. All Rights Reserved.

Warner, M., C. Mass, and E. Salathe (2012), Wintertime extreme precipitation events along the Pacific Northwest Coast: Climatology and synoptic evolution, *Mon. Weather Rev.*, *140*(7), 2021–2043.
Wood, A. W., L. R. Leung, V. Sridhar, and D. P. Lettenmaier (2004), Hydrologic implications of dynamical and statistical approaches to downscaling climate model outputs, *Clim. Change*, *62*(1), 189–216, doi:10.1023/B:CLIM.0000013685.99609.9e.
Xu, C. (1999), From GCMs to river flow: A review of downscaling methods and hydrologic modelling approaches, *Prog. Phys. Geogr.*, *23*(2), 229–249, doi:10.1177/030913339902300204.
Zhong, L., M. Li, and M. G. G. Foreman (2008), Resonance and sea level variability in Chesapeake Bay, *Cont. Shelf Res.*, *28*(18), 2565–2573.
Zijlema, M. (2010), Computation of wind-wave spectra in coastal waters with SWAN on unstructured grids, *Coastal Eng.*, *57*(3), 267–277.

© 2014. American Geophysical Union. All Rights Reserved.